JOC The Journal of Organic Chemistry

pubs.acs.org/joc Article

Synthesis and Studies of Stable Nonaromatic Dithia Pyribenzihexaphyrins

Nisha Rawat, Avisikta Sinha, Dijo Prasannan, and Mangalampalli Ravikanth*

Cite This: J. Org. Chem. 2021, 86, 6665−6673 Read Online

ABSTRACT: We report here one of the rare examples of expanded hexaphyrins named as dithia pyribenzihexaphyrin macrocycles containing six-membered rings such as pyridine and *p*-phenylene along with five-membered heterocycles such as pyrrole and thiophene as a part of a macrocyclic frame. Trifluoroacetic acid catalyzed [3 + 3] condensation of equimolar mixture of [10,10′-*bis*(*p*-*tert*-butyl phenyl)hydroxymethyl]-1,3-*bis*(2-thienyl)pyridine diol (2,6-pyri diol) and 1,4-*bis*(phenyl(1*H*-pyrrol-2-yl)methyl)-benzene (*p*-benzidipyrrane) in CH_2Cl_2 followed by oxidation with DDQ afforded stable nonaromatic dithia 2,6-pyri-*para*-benzihexapyrins **1** and **2** in 6−8% yields. The macrocycles were characterized by high-resolution mass spectroscopy and 1D and 2D NMR spectroscopy. NMR studies revealed the nonaromatic nature of dithia 2,6-pyri-*p*-benzihexaphyrins and indicated that the *para*-phenylene ring prefers to be in quininoid form rather than in benzenoid form. The macrocycles displayed sharp absorption bands in the region of ∼380−500 nm and a broad band at ∼700 nm, reflecting their nonaromatic nature. Upon protonation, these macrocycles showed NIR absorption properties. The redox studies of macrocycles indicated their electron-deficient nature. The DFT/TD-DFT studies are in line with the experimental observations.

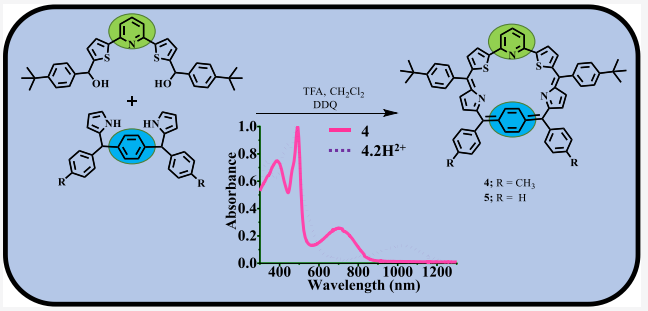

INTRODUCTION

One of the most attractive modifications of porphyrinoids is the replacement of five-membered pyrrole ring(s) with six-membered benzene, and the resulted benziporphyrinoids are known to exhibit intriguing spectroscopic, structural, and chemical properties.[1−5] Benziporphyrinoids can form stable organometallic complexes and have been shown to have applications in various fields including the development of chemical sensors and molecular recognition studies.[6−8] The characteristics of benziporphyrinoids may vary from non-aromatic[9,10] to highly aromatic[5] systems, and in a few cases, antiaromatic[11,12] structures are formed. Thus, benziporphyrinoids received a lot of attention since the aromaticity of these systems has several interesting aspects, and most notably, di-*p*-benzihexaphyrin is the first example of a Huckel−Mobius aromaticity switch.[12−15] In benziporphyrinoids, the benzene unit is connected with the rest of the porphyrinoid system either *via* its 1,3-positions[10,16] (*meta*-benziporphyrinoids) or 1,4-positions[5,12,17,18] (*para*-benziporphyrinoids). The properties of *m*-benziporphyrinoids and *p*-benziporphyrinoids are very different from each other.[3,6] The studies indicated that simple *m*-benziporphyrins are nonaromatic but can be converted into aromatic systems by suitable modifications/substitutions on the *m*-phenylene subunit,[19] whereas *p*-benziporphyrins exhibit diatropic ring current and show more aromatic features.[20] This is because, in *m*-benziporphyrins, the *m*-phenylene unit does not participate in the π delocalization of electrons with the rest of the porphyrin system, whereas, in *p*-benziporphyrins, the *p*-phenylene unit participates in the π-delocalization with the rest of the porphyrin system. Lash's[1,2,9,21,22b] and Latos-Grazynski's[5−8,11,12,22a] research groups and others[10,12,17,19,20,23,24] have extensively investigated the synthesis, properties, and coordination chemistry of *m*- and *p*-benziporphyrins. However, the reports on benzene-containing expanded porphyrinoids are relatively few to understand their physico-chemical and coordination properties.[5,6,9,12,16−20,24,25] The expanded *m*-benziporphyrinoid such as **1** was synthesized over a sequence of steps and showed its ability to act as a ligand to form organometallic complexes[24] (Chart 1).

We recently reported the synthesis of stable nonaromatic [28π] dithia *m*-benzihexaphyrins (1.0.0.1.1.1) **2** and explored their spectral and redox properties.[16] We also reported the synthesis of pyridine analogue of dithia *m*-benzihexaphyrins such as macrocycle **3** by replacing the benzene ring of dithia *m*-benzihexaphyrins **2** with 2,6-pyridine ring.[26] During the course

Received: February 22, 2021
Published: April 26, 2021

https://doi.org/10.1021/acs.joc.1c00439
J. Org. Chem. 2021, 86, 6665−6673

Chart 1. Structures of Benzihexaphyrin Analogues

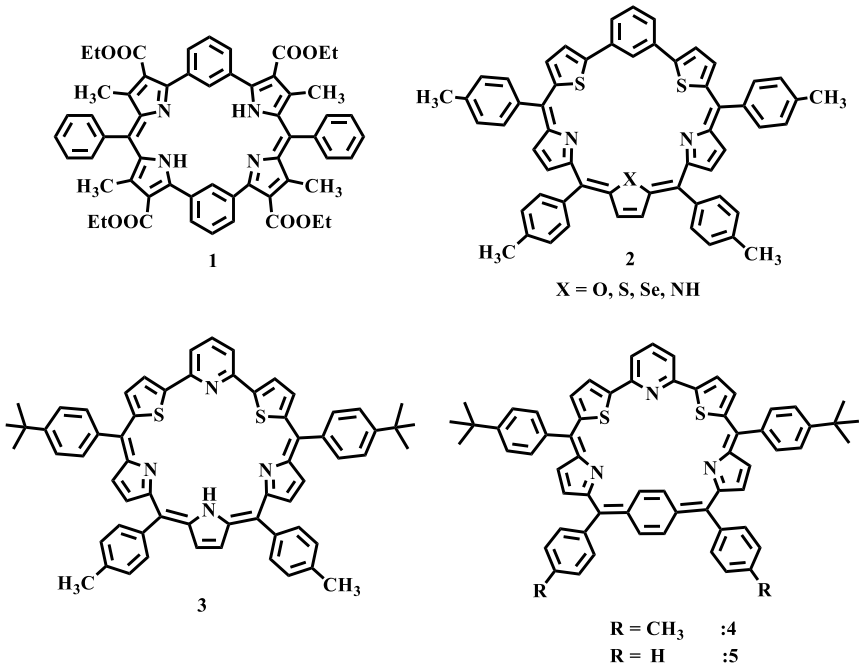

Scheme 1. Synthesis of 2,6-Pyri-dithia-*p*-benzihexaphyrins 4 and 5

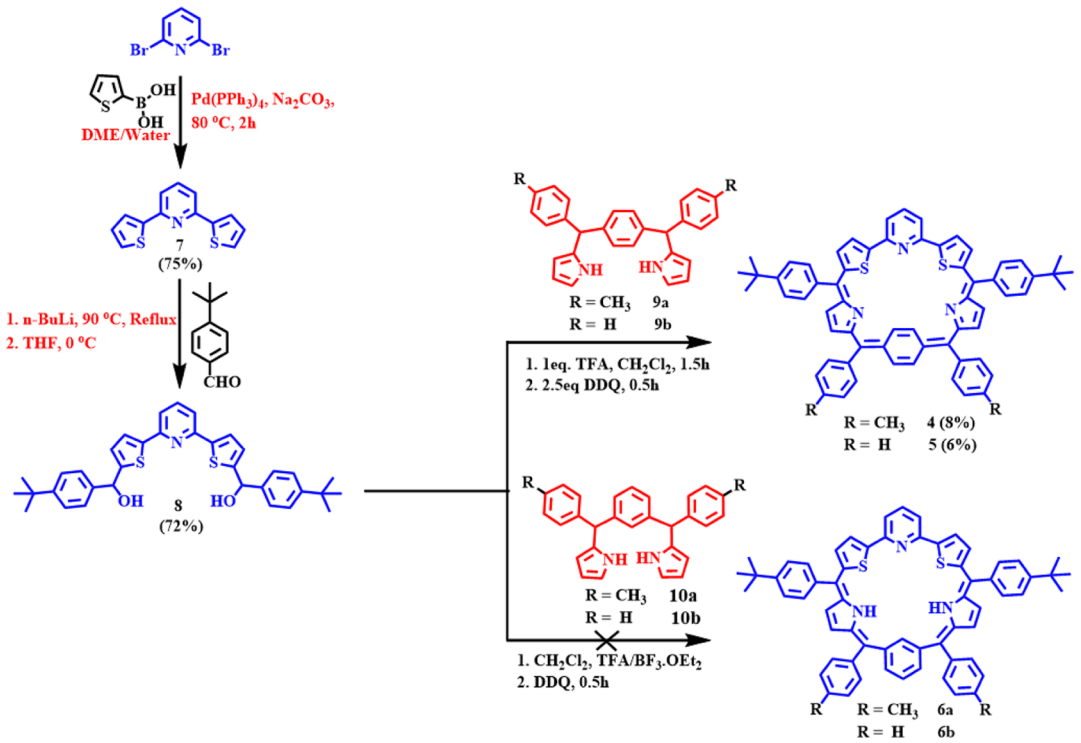

of this chemistry, we realized that it is interesting to synthesize hexaphyrins in which both benzene and pyridine units are part of the macrocyclic framework along with other five-membered heterocycles. The macrocycles consisting of different five and six membered heterocycles as a part of macrocyclic framework are very useful as ligands for selective formation of complexes with guest molecules, anions, or metal ions besides their potential applications in fields such as NIR dyes, magnetic materials, nonlinear optical materials, and so on.[21,23,27−30] A perusal of literature revealed that, to the best of our knowledge, there is only one report on porphyrinoid that contains both pyridine and *m*-phenylene rings along with other five-membered heterocycles as a part of the macrocyclic framework.[31] Herein, we report our successful synthesis of two examples of pyridine-incorporated dithia 2,6-pyri-*p*-benzihexaphyrins **4** and **5** (Chart 1) under [3 + 3] condensation reaction conditions using readily available precursors. Although macrocycles **4** and **5** are quite stable, our attempts failed when we used the other *meso*-aryl substituents such as anisyl, 2,4,6-trimethylphenyl groups adjacent to the *para*-phenylene

https://doi.org/10.1021/acs.joc.1c00439
J. Org. Chem. 2021, 86, 6665−6673

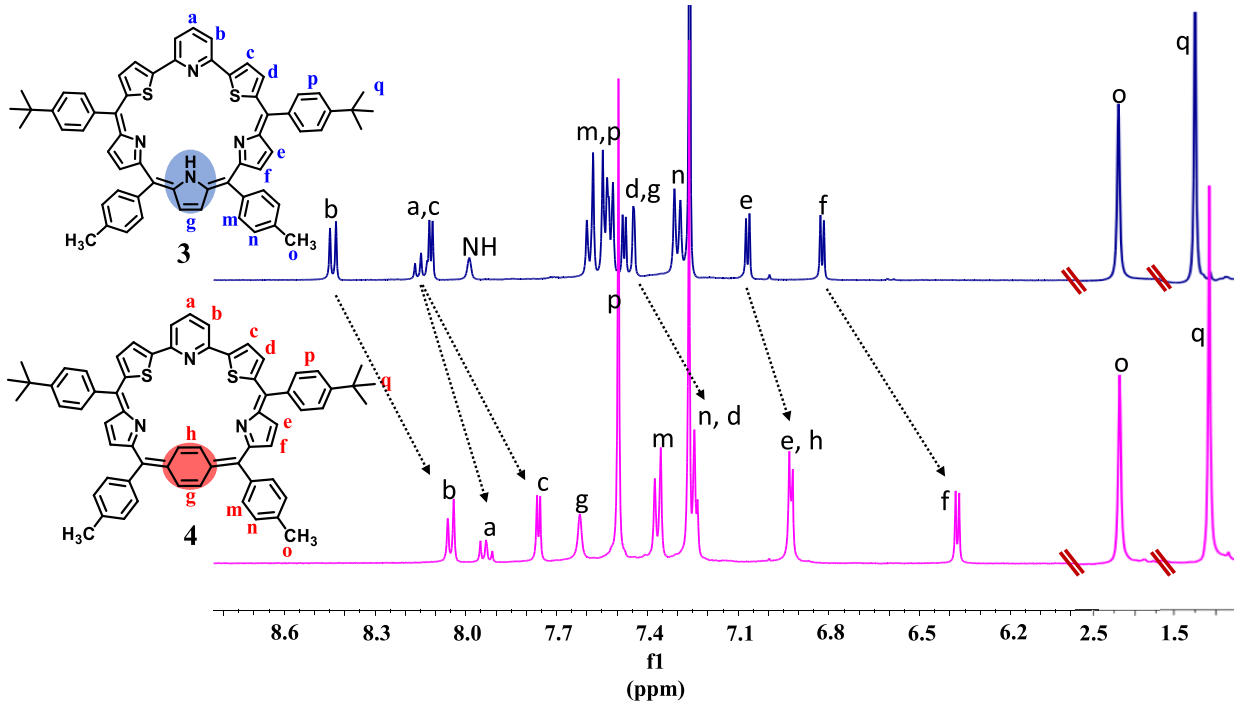

Figure 1. Comparison of ^{1}H NMR spectra of compounds **3** and **4** in $CDCl_3$ at room temperature (25 °C).

moiety[20] of hexaphyrin macrocycle. Our attempts to prepare the analogous dithia pyri *m*-benziporphyrins **6** were also unsuccessful because of their inherent unstable nature. Thus, the dithia 2,6-pyri-*p*-benzihexaphyrins **4** and **5** reported here are the only stable macrocycles that contain both pyridine and *p*-phenylene rings in their macrocyclic framework and thoroughly characterized by 1D and 2D NMR, absorption, electrochemical, and density functional theory (DFT) studies. Our studies supported the nonaromatic nature of dithia 2,6-pyri-*p*-benzihexaphyrins **4** and **5** like macrocycle **3**. However, the electronic properties are quite altered when the pyrrole ring of macrocycle **3** was replaced with *p*-phenylene ring in macrocycles **4** and **5** as reflected from their spectral and electrochemical properties.

RESULTS AND DISCUSSION

The target macrocycles **4** and **5** were synthesized as shown in Scheme 1. The desired precursor, 10,10′-*bis*(*p*-*tert*-butyl phenyl)hydroxymethyl]-1,3-*bis*(2-thienyl)pyridine diol[26] (2,6-pyri diol) **8** (Figures S1−S3), was prepared in two steps starting with commercially available 2,6-dibromopyridine. Suzuki coupling of 2,6-dibromopyridine with 4 equiv of 2-thiophene boronic acid afforded 2,6-*bis*(dithienyl)pyridine **7**. The compound **7** was treated with *n*-BuLi in THF, followed by 4-*tert*-butylbenzaldehyde, and column chromatographic purification yielded 2,6-pyri diol **8** in 72% yield. The other precursors, 1,4-*bis*(aryl(1*H*-pyrrol-2-yl)methyl)benzene (*p*-benzidipyrrane) **9a**/**9b** and 1,3-*bis*(aryl(1*H*-pyrrol-2-yl)-methyl)benzene (*m*-benzidipyrrane) **10a**/**10b**, were synthesized by following the reported synthetic procedures.[20] The 2,6-pyridine-incorporated dithia 2,6-pyri-*p*-benzihexaphyrins **4** and **5** were synthesized by the [3 + 3] condensation of equimolar mixture of 2,6-pyri diol **8** and appropriate *p*-benzidipyrrane, **9a**/**9b**, in the presence of 1 equiv of trifluoroacetic acid (TFA) in dichloromethane under an inert atmosphere for 1.5 h, followed by oxidation with 2.5 equiv of 2,3-dichloro-5,6-dicyano-1,4-benzoquinone (DDQ) in open air for 30 min at room temperature. The TLC analysis showed only one major spot corresponding to the desired macrocycles **4**/**5** as judged by high-resolution mass spectroscopy (HR-MS) analysis. The crude reaction mixture after the removal of the solvent was column chromatographed on basic alumina using petroleum ether/ethyl acetate (85:15) as an eluent to yield dithia 2,6-pyri-*p*-benzihexaphyrins, **4** and **5**, as green solids in 6−8% yields (Scheme 1). The reaction conditions were varied with different equivalents of TFA, $BF_3{\cdot}OEt_2$, and PTSA. However, no significant improvement of the yields of the dithia 2,6-pyri-*p*-benzihexaphyrins **4** and **5** were observed. Furthermore, when we used other *meso*-aryl-substituted *p*-benzidipyrranes such as anisyl and 2,4,6-trimethylphenyl-substituted *p*-benzidipyrranes for [3 + 3] condensation with *m*-pyri diol **8** under similar reaction conditions, the stable dithia 2,6-pyri-*p*-benzihexaphyrins were not formed. We also attempted the [3 + 3] condensation of 2,6-pyri diol **8** with *m*-benzidipyrranes **10a**/**10b** under various reaction conditions but failed to obtain dithia 2,6-pyri-*m*-benzihexaphyrins **6** because of the inherent unstable nature of macrocycles. Both the macrocycles **4** and **5** were freely soluble in common organic solvents. The formation of 2,6-pyri-dithia-*p*-benzihexaphyrins **4** and **5** was initially confirmed by the corresponding molecular ion in the HR-MS (Figures S4 and S7).

The 1D and 2D NMR spectroscopic techniques were used to characterize the 2,6-pyri-dithia-*p*-benzihexaphyrins **4** and **5**. Figure 1 displays the comparison of the partial ^{1}H NMR spectrum of compounds **4** and **3**. All the resonances with integrated intensities in the ^{1}H NMR spectra of **4** and **5** were identified and assigned based on their location, integration, coupling constants, and proton−proton correlations observed in ^{1}H−^{1}H COSY and ^{1}H−^{1}H NOESY NMR spectra (Figures S11 and S12, respectively). The number of resonances in the ^{1}H NMR spectra of macrocycles **4** and **5** is exactly the same as

https://doi.org/10.1021/acs.joc.1c00439
J. Org. Chem. 2021, 86, 6665−6673

Table 1. Comparison of ^{1}H NMR, Absorption, and Electrochemical Data of Compounds 4 and 5 with 3

	^{1}H NMR (δ in pm)		λ_{abs}, nm (log ε_{max})			reduction (V)		oxidation (V)		
compound	2,6-pyridine type a	protons type b	(I)	(II)	(III)	(I)	(II)	(I)	(II)	(III)
3	8.13	8.43	406 (4.2)	496 (4.5)	813 (4.0)	−0.61	−0.92	0.70	1.14	1.38
3.2H^{2+}			439 (4.4)	540 (4.5)	990 (4.0)					
4	8.05	7.93	385 (4.7)	492 (4.8)	707 (4.2)	−0.54	−0.76	0.80	0.99	1.24
4.2H^{2+}			337 (4.6)	483 (4.7)	1037 (3.8)					
5	8.06	7.93	390 (4.7)	492 (4.8)	706 (4.2)	−0.50	−0.71	0.80	1.10	1.26
5.2H^{2+}			348 (4.5)	484 (4.6)	1040 (4.2)					

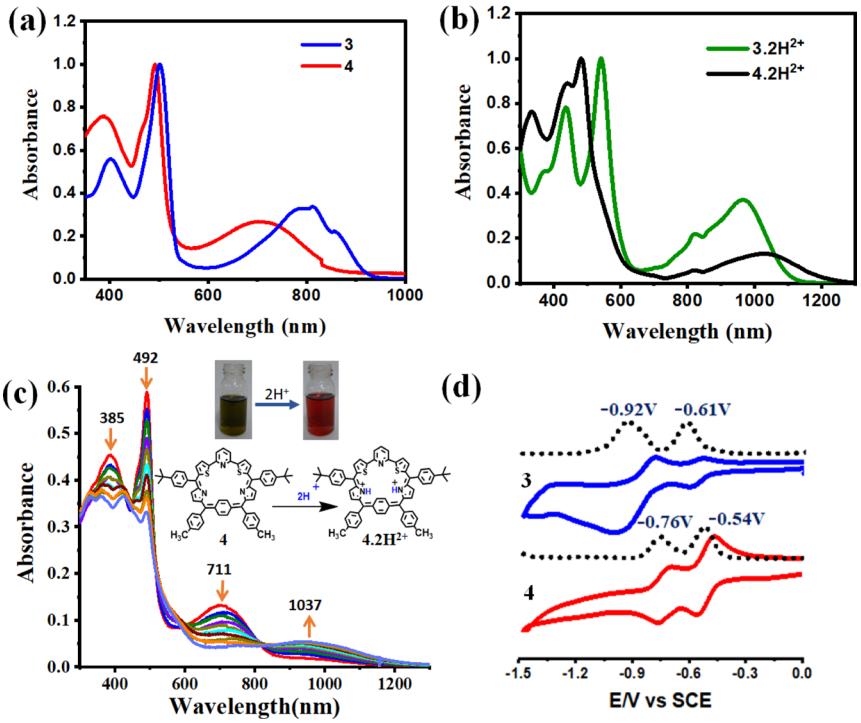

Figure 2. (a) Comparison of the normalized absorption spectra of compounds **3** and **4** in $CHCl_3$, (b) comparison of the normalized absorption spectra of compounds **3.2H^{2+}** and **4.2H^{2+}** recorded in $CHCl_3$, (c) change in the absorption spectra of **1** (1×10^{-5} M) upon the systematic addition of (1×10^{-3} M) TFA (0−10 equiv) recorded in $CHCl_3$, and (d) comparison of cyclic voltammogram (red and blue solid lines) of compounds **3** and **4**, respectively, and differential pulse voltammograms (dotted black lines) recorded in dry dichloromethane with 0.1 M TBAP as a supporting electrolyte and a saturated calomel electrode (SCE) as the reference electrode at a scan rate of 50 mV/s.

expected on the basis of their molecular structures and symmetric nature.

All the proton resonances for pyrrole, thiophene, pyridine, and benzene moieties in the macrocycle **4** appeared in the region of 6.40−8.05 ppm, indicating the nonaromatic nature[16] of compound **4**. The triplet at 7.91 ppm due to type a protons on the 2,6-pyridine ring of the macrocycle **4** showed cross-peak correlation with type b protons of the 2,6-pyridine ring protons at 8.05 ppm which appeared as a doublet. The pyridine type b protons showed NOE correlation with the doublet at 7.76 ppm, which was due to type c protons of the thiophene ring. The type c protons are cross-peak correlated with type d protons resonance at 7.24 ppm, confirming the type c and type d protons of the thiophene ring. The type d protons at 7.24 ppm of the thiophene ring show NOE correlation with type p protons of the *tert*-butyl phenyl ring at 7.50 ppm. The type p (7.50 ppm) protons are NOE correlated with type e protons of pyrrole ring resonance at 6.93 ppm which in turn is cross-peak correlated with type f proton resonance at 6.38 ppm. The type f protons at 6.38 ppm are NOE correlated with type m proton resonance at 7.37 ppm of the tolyl group which in turn was in cross-peak correlation with the type n protons resonance at 7.24 ppm. The ^{1}H NMR spectrum revealed the presence of two types of protons for the benzene ring. The inner protons, type h appeared as a doublet at 6.93 ppm, and are more upfield than the outer protons type g, which appeared as a singlet at 7.62 ppm. The type m proton showed NOE correlation with type g and type h protons clearly confirming the structure. The absence of a −NH proton also reveals that the macrocycle has a structure with a "quinonoid" form rather than benzenoid. To understand the alteration in electronic properties when the pyrrole ring in macrocycle **3** is replaced with the *p*-phenylene ring in macrocycle **4**, we compared the ^{1}H NMR spectra of macrocycle **3** and **4** in the selected region as shown in Figure 1. As clear from the Figure 1, all the outer ring protons of macrocycle **4** experienced upfield shifts compared to macrocycle **3**. For example, the pyridine protons (type a and type b) which appeared as resonances at 8.13 and 8.43 ppm in macrocycle **3** experienced upfield shifts in macrocycle **4** and appeared at 7.93 and 8.05 ppm, respectively. Similarly, the pyrrole ring protons (type e and type f) which appeared at 7.07 and 6.82 ppm in macrocycle **3** were upfield shifted to 6.93 and

https://doi.org/10.1021/acs.joc.1c00439
J. Org. Chem. 2021, 86, 6665−6673

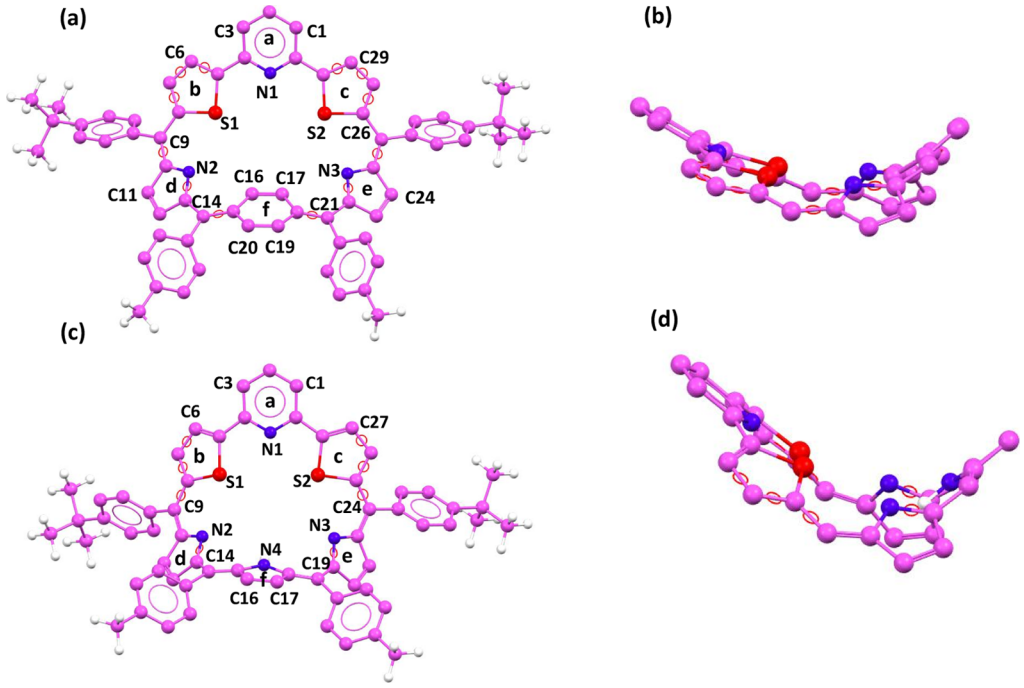

Figure 3. Optimized geometries of compound **4:** (a) top view and (b) side view; compound **3:** (c) top view and (d) side view. The phenyl rings are omitted for clarity in the side view.

6.38 ppm, respectively, in macrocycle **4**. The thiophene protons (type c and type d) also shifted to upfield in macrocycle **4** compared to macrocycle **3**. All these changes in the chemical shifts of various protons of macrocycle clearly supports the alteration in ring current upon replacing the five-membered pyrrole ring in macrocycle **3** with six-membered *p*-phenylene ring in macrocycle **4**.

Absorption and Electrochemical Properties. The absorption spectra of macrocycles **4** and **5** and their protonated derivatives **4.2H**$^{2+}$ and **5.2H**$^{2+}$ were recorded in chloroform and compared with macrocycle **3** and its protonated derivative **3.2H**$^{2+}$ (Table 1). The comparison of absorption spectra of **3** and **4** is presented in Figure 2a and the protonated derivatives **3.2H**$^{2+}$ and **4.2H**$^{2+}$ in Figure 2b (Table 1). Due to their nonaromatic characteristic, 2,6-pyri-dithia-*p*-benzihexaphyrins **4** and **5** showed two sharp absorptions in the region of 380−500 nm and a broad band at ∼700 nm (Figure 2). The absorption spectral pattern of macrocycles **4** and **5** resembles closely to that of dithia 2,6-pyrihexaphyrin macrocycle[26] **3** with changes in their peak maxima. Upon protonation of macrocycles **4** and **5** with TFA, the intensity of the broad band at ∼700 nm was decreased along with the appearance of a new broad band at 1030 nm due to the formation of protonated derivatives **4.2H**$^{2+}$ and **5.2H**$^{2+}$. These absorption features were also similar to that of the protonated derivative **3.2H**$^{2+}$ with significant shifts in their absorption peak maxima.[26] All these absorption spectral shifts support the alteration of electronic properties in dithia 2,6-pyri-*p*-benzihexaphyrins **4** and **5** compared to dithia 2,6-pyrihexaphyrin **3**.

We also carried out the systematic protonation studies by the addition of increasing equivalents of TFA to macrocycle **4** in $CHCl_3$ as shown in Figure 2c. Upon increasing addition of TFA (0−10 equiv) to compound **4** in chloroform, the color of the solution was changed from green to red due to the formation of protonated macrocycle **4.2H**$^{2+}$. In protonated macrocycle **4.2H**$^{2+}$, the peak intensity at 385 nm was decreased and blue-shifted to 337 nm; the intensity of the peak at 492 nm was also decreased and blue-sifted to 483 nm along with the appearance of a new shoulder band at 443 nm and the peak at 707 nm was diminished gradually and a new broad band appeared in the NIR region with peak maxima at 1037 nm along with two clear isosbestic points at 597 and 820 nm supporting the formation of protonated macrocycle **4.2H**$^{2+}$.

The redox properties of compounds **4** and **5** along with **3** were probed using cyclic and differential pulse voltammetry (DPV) at a scan rate of 50 mV/s using tetra-*n*-butylammonium perchlorate as the supporting electrolyte and SCE as the reference electrode (Figure S15). All the potentials were calibrated by using ferrocene as an external standard and comparison of reduction waves of compound **3** and **4** is shown in Figure 2d. Similar to recently reported dithia 2,6-pyrihexaphyrin **3**,[26] the compound **4** showed three irreversible oxidations (0.80, 0.99, and 1.24 V) and two reversible reduction peaks at −0.76 and −0.54 V (Table 1). Thus, the redox data indicates that the macrocycles **4** and **5** were easier to reduce than that of previously reported dithia 2,6-pyrihexaphyrin[26] **3** (−0.92 and −0.61 V) supporting their electron-deficient nature.

Theoretical Studies. The ground-state geometry optimization at the DFT level and nucleus-independent chemical shifts (NICS)[32] calculations for compound **4** were performed by using the B3LYP/6-31G (d, p) level to probe into the structural, spectral, and the electrochemical properties. Figure 3 presents the optimized geometries of the macrocycles **3** and **4**. It is clearly visible from Figure 3 that the macrocycles **3** and **4** adopt a highly distorted saddle-shaped conformation. This feature supports the nonplanar geometry of macrocycles **3** and **4**. The highly contorted structure of macrocycle **4** was very well evident from the angle of deviations of the heterocycle and benzene rings present inside the macrocyclic core. In macrocycle **4**, the pyridine unit (ring a) was found to be

https://doi.org/10.1021/acs.joc.1c00439
J. Org. Chem. 2021, 86, 6665−6673

deviated by an angle of 50.02° w.r.t the "mean plane" defined by the four *meso* carbon atoms (C9, C14, C21, and C26). The two thiophene rings (ring b and ring c) connected at the 2,5 position of "ring a" exhibits almost a similar magnitude of deviation wherein the thiophene ring (ring b) bends away from the "mean plane" by an angle of 35.55° and the other thiophene ring (ring c) by an angle of 36.26° (Table 2). A similar trend in the angle of deviation was displayed by the two pyrrole rings (ring d and e) which were oriented below the "mean plane". Among all the rings which were a part of the macrocycle, the deviation exerted by the phenylene ring (ring f) was found to be the least (18.6°).

Table 2. Comparison of Various Bond Angles

deviation from the mean plane	compound **3** (deg)	compound **4** (deg)
ring a	51.28	50.02
ring b	46.13	35.55
ring c	52.45	36.26
ring d	41.43	34.38
ring e	56.58	35.41
ring f	24.18	18.6

In macrocycle **3**, where the five-membered pyrrole ring (ring f) is present in the place of a six-membered phenylene ring (ring f), the overall distortion in the macrocycle markedly increases which is reflected in the increased angle deviation of all the rings w.r.t the "mean plane" defined by the four *meso* carbon atoms (C9, C14, C19, and C24) (Table 2). The pyrrole ring (ring f) was deviated by an angle of 24° w.r.t "mean plane" as a result of which the benzidipyrrane half of the molecule adopts an oval shape. The nitrogen atoms (N2 and N3) of the pyrrole ring in the macrocycle **4** were situated at a distance of 0.138 Å and 0.131 Å, respectively, whereas the nitrogen atom (N1) of the pyridine ring was placed at a distance of 2.280 Å from the "mean plane". The sulfur atoms of the thiophene rings were located at a distance of 1.205 Å, whereas the C atoms of the benzene ring (ring f) displayed little to almost no deviation (0.679−0.89 Å). On the other hand, in macrocycle **3**, the N atom of the pyridine ring was located at a distance of 3.121 Å which is greater than that observed for macrocycle **4**. Similarly, the nitrogen atoms of the pyrrole rings N2, N3, and N4 were also deviated to a greater extent in macrocycle **3**, which further supports the enhanced nonplanarity and distortion of macrocycle **3** compared to macrocycle **4**.

The close bond length analysis indicates that the C16−C17 (1.365 Å) and C19−C20 (1.359 Å) bond lengths of the *p*-phenylene ring (f) were relatively shorter as opposed to those of C15−C16, C17−C18, C18−C19, and C20−C15 (1.446 ± 0.02 Å), which displayed almost a single-bond characteristic. This feature of nonequivalent bond lengths in the *p*-phenylene ring of macrocycle **4** is very much unlike free benzene which shows identical bond lengths (1.40 Å). These values clearly indicate that the double bond characteristic exists between C16−C17 and C19−C20, whereas C15−C16, C17−C18, C18−C19, and C20−C15 are nearly single bond in nature. However, the C−C and C−N bond lengths in pyridine (ring a) and pyrrole (ring d and ring e) in macrocycle **4** were comparable to the bond lengths in free pyrrole and pyridine. The bond length equalization of the *p*-phenylene ring is one of the parameters that defines its aromaticity. Thus, the absence of equal bond length of the *p*-phenylene ring inside the macrocyclic core clearly highlights its nonaromatic characteristic. On the contrary, for macrocycle **3**, the C−C and C−N bond lengths of the pyrrole moiety (rings d, e, and f) were slightly elongated as compared to free pyrrole, whereas for the pyridine ring, the bond lengths were almost comparable.

The analysis of the selected Frontier molecular orbital reveals that for compound **4**, the highest occupied molecular orbital (HOMO) represents nonuniform distribution of orbital density, which is mostly focused on the benzidipyrrane moiety with very less orbital density on the meso substituents, whereas lowest unoccupied molecular orbital (LUMO) presents a very uniform distribution of orbital density throughout the macrocyclic framework, leaving no electron density on the *meso* aryl substituents. Figure 4 illustrates the comparison of orbital energies of HOMO and LUMO along with their band gap (expressed in eV) for macrocycles **3** and **4**. Macrocycle **3** also exhibits similar orbital density distribution in HOMO and

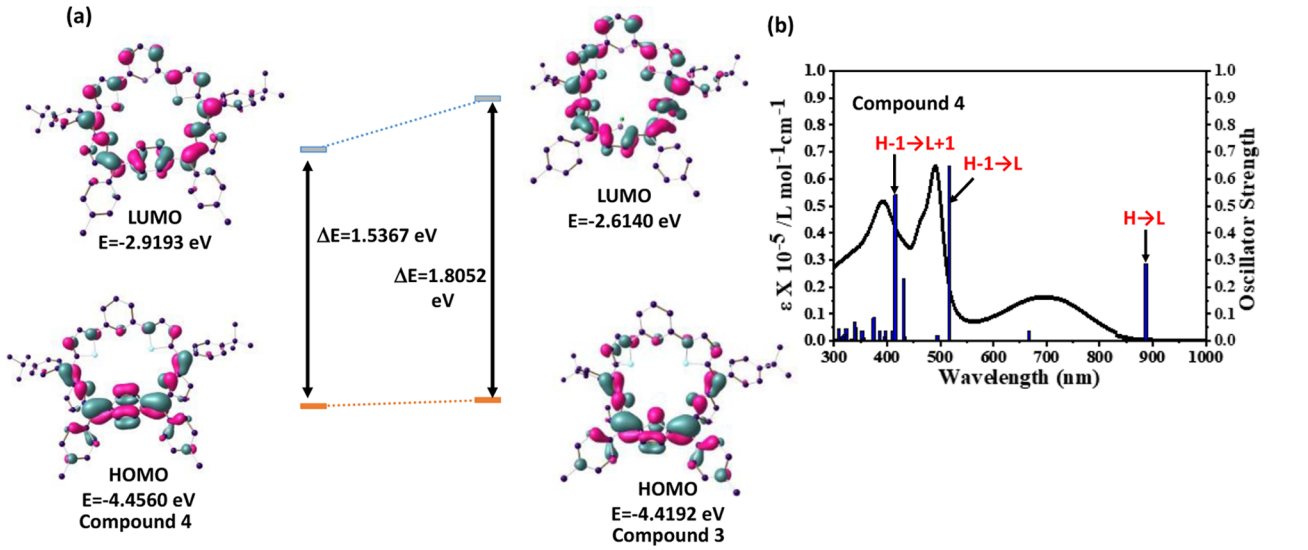

Figure 4. (a) Energy-level diagram (selected FMOs) of compounds **4** and **3** calculated by the B3LYP/6−31g(d, p) method and (b) calculated excitations (blue vertical lines) and experimental UV/vis absorption spectra (black line) for compound **4** (ε in M^{-1} cm^{-1}).

https://doi.org/10.1021/acs.joc.1c00439
J. Org. Chem. 2021, 86, 6665−6673

LUMO to macrocycle **4**. The very even distribution of orbital density throughout the macrocyclic core over the heterocyclic and *p*-phenylene rings for compound **4** via the *meso* sp^2 carbon atoms support the effective π overlap along the predicted conjugation pathway.

As clearly shown in Figure 4, the presence of a six-membered *p*-phenylene ring in the place of a five-membered pyrrole ring in macrocycle **4** stabilizes the LUMO because of which the HOMO−LUMO band gap also undergoes a notable decrease from ΔE = 1.8053 eV in macrocycle[26] **3** to ΔE = 1.5367 eV in macrocycle **4**, but both these macrocycles show comparable absorption features. The HOMO−LUMO gap (1.5367 eV) in macrocycle **4** matches well with the experimentally computed value from the cyclic voltammetric study (Table S1). Thus, the spectral and electrochemical properties predicted by DFT are consistent with the experimental data.

Furthermore, the TD-DFT studies were also performed to predict the oscillator strength and excitation energies of the first S_0−S_n transitions. The calculated vertical excitation energies for macrocycle **4** fairly matched with their respective experimental data both in position and in relative intensity. In the case of compound **4** (Figure 4b), the absorption/excitations around the region of 390−410 and ∼500 nm with large oscillator strengths originating mainly from HOMO − 1 → LUMO + 1 and HOMO − 1 → LUMO transitions, respectively, while the broad band of low intensity in the region of 700−900 nm arises from the HOMO → LUMO transition. However, for macrocycle[26] **3**, the HOMO → LUMO + 2 transitions were responsible for the sharp intense band around 410 nm and the low energy charge transfer band was mainly a consequence of the HOMO → LUMO transitions. Upon protonation, the HOMO−LUMO band gap for both the compounds $\mathbf{3.2H^{2+}}$ and $\mathbf{4.2H^{2+}}$ showed a significant decrease in energy (ΔE = 1.2263 eV for $\mathbf{4.2H^{2+}}$ and 1.4829 eV for $\mathbf{3.2H^{2+}}$) as compared to their corresponding free bases **4** and **3**, respectively, which justifies the observed bathochromic shifts in the absorption spectra (Figure S18).

The ^{1}H chemical shifts of compound **4** were simulated using the gauge-including atomic orbital method at the B3LYP/6-311G(d,p) level. The ^{1}H chemical shift values were calculated with reference to $CHCl_3$ (7.26 ppm). The simulated ^{1}H NMR was qualitatively in good agreement with the experimentally recorded ^{1}H NMR spectrum in $CDCl_3$ (Figure 1). The experimental and theoretical chemical shifts are presented in the Supporting Information (Tables S2 and S3), for example, the *para*-phenylene protons of macrocycle **4**, the type h and type g observed at 6.93 and 7.62 ppm in the ^{1}H NMR spectrum appeared at 7.03 and 7.26, respectively, in the theoretically computed spectrum.

For the quantitative evaluation of aromaticity, the NICS[33] and harmonic oscillator model of aromaticity (HOMA)[34] values were calculated for macrocycle **4**. The isotropic NICS $(NICS(0)_{iso})$ and the zz component of the shielding tensor $(NICS(0)_{zz})$ values in the S_0 state for the compound **4** are −0.6220 and +4.5369, respectively, suggesting its nonaromatic nature.[35−38] Thus, the molecule lacks both local and ground-state global aromaticity. The HOMA indices were calculated[39] along various π-conjugation paths using the optimized structure for macrocycle **4**. The HOMA factor is 0 for a model nonaromatic ring and 1 for a system where there is complete delocalization. The HOMA values of macrocycle **4** range from −0.26 to 0.47 (Figure S19). It has been reported that for rings consisting of localized single and double bonds, very small and negative HOMA values are obtained, suggesting its nonaromatic nature.[38,39]

Thus, the spectral and electrochemical properties predicted by DFT agreed closely with the experimental data. In short, the absence of bond length equalization, low-field ^{1}H NMR shifts, small NICS values, and nonplanar structure[40] undoubtedly supports the nonaromatic nature of macrocycle **4**.

CONCLUSIONS

In summary, we have successfully synthesized the stable nonaromatic 2,6-pyri-dithia-*p*-benzihexaphyrins **4** and **5** using-[3 + 3] condensation reaction with the readily available precursors. To the best of our knowledge, compounds **4** and **5** represent one of the limited examples of the pyridine-incorporated dithia *para*-benzihexaphyrins. The nonaromatic features of the macrocycles were revealed by absorption and NMR studies. The experimental results were further supported by DFT studies. We anticipate that the presence of pyridine/pyrrole nitrogens, *p*-phenylene carbons, and thiophene sulfurs would help to form interesting coordination compounds and such studies are underway.

EXPERIMENTAL SECTION

General Experimental Section. All the chemicals used for the synthesis were of reagent grade unless otherwise specified. Boron trifluoride diethyl etherate ($BF_3{\cdot}OEt_2$), TFA, and 2,3-dichloro-5,6-dicyano-1,4-benzoquinone (DDQ) obtained from Sigma-Aldrich were used as such. All other chemicals used for the synthesis were of reagent grade unless otherwise specified. The 2,6-pyri diol **8** (10,10′-*Bis*[4-(*tert*-butyl)phenyl]-1,3-*bis*(2-thienyl)-pyridinediol) was prepared by following our reported procedure.[26] Solvents such as petroleum ether (60−80 °C), ethyl acetate, and dichloromethane purchased from Merck, India, were used without further purification. Column chromatography was performed on basic alumina (80−200 mesh). ^{1}H (1D and 2D) and $^{13}C\{^1H\}$ NMR spectra were recorded on a Bruker 400 and 500 MHz FT-NMR spectrometer in $CDCl_3$ using tetramethylsilane as the internal reference. The $^{13}C\{^1H\}$ NMR frequencies are 125.77 and 100.06 MHz for 500 and 400 MHz instruments, respectively. Structural assignments were made with additional information from ^{1}H−^{1}H COSY and ^{1}H−^{1}H NOESY experiments. The high-resolution mass spectroscopy (HR-MS) spectra were recorded with a Bruker maXis Impact and QTof micro mass spectrometer using positive mode ESI methods in acetonitrile or methanol. UV−visible absorption spectra were recorded on a Cary Series UV−vis−NIR and a UV 3600 Shimadzu spectrophotometer. The stock solutions of the compounds (5×10^{-4} M) were prepared using HPLC-grade chloroform. Cyclic voltammetric studies were carried out with a BAS electrochemical system utilizing the three-electrode configuration consisting of glassy carbon (working electrode), platinum wire (auxiliary electrode), and saturated calomel (reference electrode) electrodes. The concentrations of the samples were maintained as 0.01 M containing tetrabutylammonium perchlorate (TBAP) as the supporting electrolyte (0.1 M) in dichloromethane at 25 °C under an argon atmosphere at a scan rate of 50 mV/s. The half-wave potentials measured using DPV were calculated manually by taking the average of the cathodic and anodic peak potentials. All the potentials were calibrated by using ferrocene as an external standard, taking $E_{1/2}$ (Fc/Fc^+) = 0.42 V versus SCE.

All the theoretical calculations utilized 6-31g(d,p) level of theory and were performed using the Gaussian09 package. The ground-state geometry optimization, NICS,[32] and AICD calculations for the compounds **4** and **5** were performed at the DFT level using Becke's three-parameter functional combined with the Lee−Yang−Parr exchange correlation functional (B3LYP).

Compound 4. To a solution of 1,3-*bis*(2-thienyl)-pyridinediol[26] (100 mg, 0.176 mmol) and 1,4-bis(*p*-tolyl(2-pyrolyl)methyl)

https://doi.org/10.1021/acs.joc.1c00439
J. Org. Chem. 2021, 86, 6665−6673

benzene[20] (73.36 mg, 0.176 mmol) dissolved in 200 mL of CH_2Cl_2 under an inert atmosphere, TFA (13 μL, 0.176 mmol) was added and stirred for 1.5 h. DDQ (99.95 mg, 0.440 mmol) was then added to the reaction mixture and stirred for an additional 0.5 h in open air. The solvent was removed under reduced pressure, and the crude compound was subjected to basic alumina column chromatography. The desired product was isolated using petroleum ether/ethyl acetate (85:15) as a green solid in 8% yield (14 mg); mp > 300 °C; ^{1}H NMR (400 MHz, $CDCl_3$): δ 8.05 (d, J = 7.8 Hz, 2H), 7.93 (t, 1H), 7.76 (d, J = 4.2 Hz, 2H), 7.62 (s, 2H), 7.50 (s, 8H), 7.37 (d, J = 7.9 Hz, 4H), 7.24 (d, J = 4.2 Hz, 6H), 6.93 (d, J = 4.5 Hz, 4H), 6.38 (d, J = 4.6 Hz, 2H), 2.44 (s, 6H), 1.42 (s, 18H); ^{13}C{^{1}H} NMR (101 MHz, $CDCl_3$): δ 169.6, 154.5, 153.5, 151.9, 144.2, 142.5, 138.4, 137.6, 137.1, 137.0, 135.7, 134.2, 132.6, 132.1, 131.7, 130.9, 129.7, 128.5, 126.0, 125.2, 124.5, 118.16, 34.8, 31.4, 21.4; UV−vis: $CHCl_3$, λ_{max}/nm (log ε) 385(4.7), 492(4.8), 707(4.2); HR-MS (ESI-TOF) m/z: [M + H]$^+$ calcd for $C_{65}H_{56}N_3S_2$, 942.3919; found, 942.3910.

Compound 5. Green solid. Yield 6% (10 mg)); mp > 300 °C; ^{1}H NMR (400 MHz, $CDCl_3$): δ 8.06 (d, J = 7.8 Hz, 2H), 7.93 (t, 1H), 7.77 (d, J = 4.1 Hz, 2H), 7.67 (s, 2H), 7.50 (s, 8H), 7.47−7.40 (m, 10H), 7.25 (d, 2H), 6.95−6.87 (m, 4H), 6.35 (d, J = 4.6 Hz, 2H), 1.42 (s, 18H); ^{13}C{^{1}H} NMR (101 MHz, $CDCl_3$): δ 169.4, 154.5, 153.6, 151.9, 151.5, 144.1, 142.8, 141.4, 137.0, 136.3, 135.8, 135.4, 134.3, 132.4, 132.1, 131.6, 130.9, 127.9, 127.7, 125.3, 124.5, 118.2, 34.8, 31.4; UV−vis: $CHCl_3$, λ_{max}/nm (log ε) 390(4.7), 492(4.8), 706 (4.2); HR-MS (ESI-TOF) m/z: [M + H]$^+$ calcd for $C_{63}H_{52}N_3S_2$, 914.3597; found, 914.3592.

■ ASSOCIATED CONTENT

Supporting Information

The Supporting Information is available free of charge at https://pubs.acs.org/doi/10.1021/acs.joc.1c00439.

HR-MS, ^{1}H, ^{13}C{^{1}H}, 2D NMR, absorption and electrochemical data, and DFT studies (PDF)

■ AUTHOR INFORMATION

Corresponding Author

Mangalampalli Ravikanth − *Indian Institute of Technology, Mumbai 400076, India;* orcid.org/0000-0003-0193-6081; Phone: 91-22-5767176; Email: ravikanth@chem.iitb.ac.in; Fax: 91-22-5723480

Authors

Nisha Rawat − *Indian Institute of Technology, Mumbai 400076, India*

Avisikta Sinha − *Indian Institute of Technology, Mumbai 400076, India*

Dijo Prasannan − *Indian Institute of Technology, Mumbai 400076, India*

Complete contact information is available at: https://pubs.acs.org/10.1021/acs.joc.1c00439

Notes

The authors declare no competing financial interest.

■ ACKNOWLEDGMENTS

M.R. acknowledges the financial support from Science & Engineering Research Board (SERB), Govt. of India. N.R. thanks University Grants Commission, Govt. of India; A.S. and D.P. thanks IIT Bombay for the Institute Fellowship.

■ REFERENCES

(1) Lash, T. D. Recent Advances on the Synthesis and Chemistry of Carbaporphyrins and Related Porphyrinoid Systems. *Eur. J. Org. Chem.* **2007**, 5461−5481.

(2) Lash, T. D. Benziporphyrins, a Unique Platform for Exploring the Aromatic Characteristics of Porphyrinoid Systems. *Org. Biomol. Chem.* **2015**, *13*, 7846−7878.

(3) Stępień, M.; Latos-Grazyński, L. Benziporphyrins: Exploring Arene Chemistry in a Macrocyclic Environment. *Acc. Chem. Res.* **2005**, *38*, 88−98.

(4) Lash, T. D. Carbaporphyrinoid Systems. *Chem. Rev.* **2017**, *117*, 2313−2446.

(5) Stępień, M.; Latos-Grazyński, L. Tetraphenyl-p-Benziporphyrin: A Carbaporphyrinoid with Two Linked Carbon Atoms in the Coordination Core. *J. Am. Chem. Soc.* **2002**, *124*, 3838−3839.

(6) Stępień, M.; Latos-Grazyński, L.; Szterenberg, L.; Panek, J.; Latajka, Z. Cadmium(II) and Nickel(II) Complexes of Benziporphyrins. A Study of Weak Intramolecular Metal-Arene Interactions. *J. Am. Chem. Soc.* **2004**, *126*, 4566−4580.

(7) Idec, A.; Pawlicki, M.; Latos-Grażyński, L. Ruthenium(II) and Ruthenium(III) Complexes of p-Benziporphyrin: Merging Equatorial and Axial Organometallic Coordination. *Inorg. Chem.* **2017**, *56*, 10337−10352.

(8) Hurej, K.; Pawlicki, M.; Latos-Grażyński, L. Rhodium-Induced Reversible C−C Bond Cleavage: Transformations of Rhodium(III) 22-Alkyl-m -benziporphyrins. *Chem.—Eur. J.* **2018**, *24*, 115−126.

(9) Lash, T. D.; Toney, A. M.; Castans, K. M.; Ferrence, G. M. Synthesis of Benziporphyrins and Heterobenziporphyrins and an Assessment of the Diatropic Characteristics of the Protonated Species. *J. Org. Chem.* **2013**, *78*, 9143−9152.

(10) Berlin, K.; Breitmaier, E. Benziporphyrin, a Benzene-Containing, Nonaromatic Porphyrin Analogue. *Angew. Chem., Int. Ed. Engl.* **1994**, *33*, 1246−1247.

(11) Idec, A.; Pawlicki, M.; Latos-Grażyński, L. Three-Stage Aromaticity Switching in Boron(III) and Phosphorus(V) N-Fused p -Benziporphyrin. *Chem.—Eur. J.* **2019**, *25*, 200−204.

(12) Stępień, M.; Szyszko, B.; Latos-Grazyński, L. Steric Control in the Synthesis of P-Benziporphyrins. Formation of a Doubly n-Confused Benzihexaphyrin Macrocycle. *Org. Lett.* **2009**, *11*, 3930−3933.

(13) Stępień, M.; Latos-Grażyński, L.; Sprutta, N.; Chwalisz, P.; Szterenberg, L. Expanded Porphyrin with a Split Personality: A Hückel−Möbius Aromaticity Switch. *Angew. Chem.* **2007**, *119*, 8015−8019.

(14) Szyszko, B.; Sprutta, N.; Chwalisz, P.; Stępień, M.; Latos-Grażyński, L. Hückel and Möbius Expandedpara-Benziporphyrins: Synthesis and Aromaticity Switching. *Chem.—Eur. J.* **2014**, *20*, 1985−1997.

(15) Yoon, Z. S.; Osuka, A.; Kim, D. Möbius aromaticity and antiaromaticity in expanded porphyrins. *Nat. Chem.* **2009**, *1*, 113−122.

(16) Kumar, S.; Ravikanth, M. Synthesis of Stable [28π] m-Benzihexaphyrins (1.0.0.1.1.1). *J. Org. Chem.* **2017**, *82*, 12359−12365.

(17) Sreedhar Reddy, J.; Anand, V. G. π-Conjugated macrocycles from thiophenes and benzenes. *Chem. Commun.* **2008**, 1326−1328.

(18) Jeong, S.-D.; Park, K. J.; Kim, H.-J.; Lee, C.-H. Meso-Alkylidenyl-Thia(p-Benzi)Porphyrins and Their Unusual Protonation Selectivity. *Chem. Commun.* **2009**, 5877−5879.

(19) Sengupta, R.; Thorat, K. G.; Ravikanth, M. Effects of Core Modification on Electronic Properties of Para-Benziporphyrins. *Inorg. Chem.* **2019**, *58*, 12069−12082.

(20) Sengupta, R.; Thorat, K. G.; Ravikanth, M. Synthesis of Nonaromatic and Aromatic Dithia Benzisapphyrins. *J. Org. Chem.* **2018**, *83*, 11794−11803.

(21) Lash, T. D.; Chaney, S. T. Oxypyriporphyrin, the First Fully Aromatic Porphyrinoid Macrocycle with a Pyridine Subunit. *Chem.—Eur. J.* **1996**, *2*, 994−998.

(22) (a) Myśliborski, R.; Latos-Grazyński, L. Carbaporphyrinoids Containing a Pyridine Moiety: 3-Aza-Meta-Benziporphyrin and 24-Thia-3-Aza-Meta-Benziporphyrin. *Eur. J. Org. Chem.* **2005**, 5039−5048. (b) Lash, T. D.; Pokharel, K.; Yant, V. R.; Ferrence, G. M.; Ferrence, G. M. Aromatic and Nonaromatic Pyriporphyrins†. *Org. Lett.* **2007**, *9*, 2863−2866.

(23) Das, M.; Chitranshi, S.; Murugavel, M.; Adinarayana, B.; Suresh, C. H.; Srinivasan, A. Isosmaragdyrin with an N3C2 core: stabilization of Rh(i) and organo-Pt(ii) complexes. *Chem. Commun.* **2020**, *56*, 3551−3554.
(24) Setsune, J.-i.; Toda, M.; Yoshida, T.; Imamura, K.; Watanabe, K. The Synthesis and Dynamic Structures of Multinuclear Complexes of Large Porphyrinoids Expanded by Phenylene and Thienylene Spacers. *Chem.—Eur. J.* **2015**, *21*, 12715−12727.
(25) Hong, S.-J.; Dutta, R.; Kumar, R.; He, Q.; Lynch, V. M.; Sessler, J. L.; Lee, C.-H. meso-Alkylidenyl dibenzihexaphyrins: synthesis and protonation studies. *Chem. Commun.* **2019**, *55*, 9693−9696.
(26) Rawat, N.; Thorat, K. G.; Kumar, S.; Ravikanth, M. Synthesis of Expanded Hetero 2,6-Pyrihexaphyrins. *Eur. J. Org. Chem.* **2020**, 736−743.
(27) Das, B.; McPherson, J. N.; Colbran, S. B. Oligomers and macrocycles with [m]pyridine[n]pyrrole (m + n ≥ 3) domains: Formation and applications of anion, guest molecule and metal ion complexes. *Coord. Chem. Rev.* **2018**, *363*, 29−56.
(28) Mori, D.; Yoneda, T.; Suzuki, M.; Hoshino, T.; Neya, S. meso -Diketopyripentaphyrin and Diketopyrihexaphyrin as Macrocyclic Tripyrrinone Ligands for Ni II Ions. *Chem.—Asian J.* **2019**, *14*, 4169−4173.
(29) Sim, E.-K.; Jeong, S.-D.; Yoon, D.-W.; Hong, S.-J.; Kang, Y.; Lee, C.-H. Porphyrins Bearing Stablemeso-Alkylidenyl Double Bonds. A New Family of Nonplanar Porphyrinoids. *Org. Lett.* **2006**, *8*, 3355−3358.
(30) Neya, S.; Suzuki, M.; Mochizuki, T.; Hoshino, T.; Kawaguchi, A. T. Porphyrinoid Aromaticity Induced by the Interaction between Oxidized and Reduced Pyridine Subunits. *Eur. J. Org. Chem.* **2015**, 3824−3829.
(31) Setsune, J.-I.; Watanabe, K. Cryptand-like Porphyrinoid Assembled with Three Dipyrrylpyridine Chains: Synthesis, Structure, and Homotropic Positive Allosteric Binding of Carboxylic Acids. *J. Am. Chem. Soc.* **2008**, *130*, 2404−2405.
(32) Stanger, A. Nucleus-Independent Chemical Shifts (NICS): Distance Dependence and Revised Criteria for Aromaticity and Antiaromaticity. *J. Org. Chem.* **2006**, *71*, 883−893.
(33) Chen, Z.; Wannere, C. S.; Corminboeuf, C.; Puchta, R.; Schleyer, P. v. R. Nucleus-Independent Chemical Shifts (NICS) as an Aromaticity Criterion. *Chem. Rev.* **2005**, *105*, 3842−3888.
(34) Krygowski, T. M.; Szatylowicz, H.; Stasyuk, O. A.; Dominikowska, J.; Palusiak, M. Aromaticity from the Viewpoint of Molecular Geometry: Application to Planar Systems. *Chem. Rev.* **2014**, *114*, 6383−6422.
(35) Peeks, M. D.; Gong, J. Q.; McLoughlin, K.; Kobatake, T.; Haver, R.; Herz, L. M.; Anderson, H. L. Aromaticity and Antiaromaticity in the Excited States of Porphyrin Nanorings. *J. Phys. Chem. Lett.* **2019**, *10*, 2017−2022.
(36) Mills, N. S.; Llagostera, K. B. Summation of Nucleus Independent Chemical Shifts as a Measure of Aromaticity. *J. Org. Chem.* **2007**, *72*, 9163−9169.
(37) Schleyer, P. V. R.; Maerker, C.; Dransfeld, A.; Jiao, H.; Van Eikema Hommes, N. J. R. Nucleus-Independent Chemical Shifts: A Simple and Efficient Aromaticity Probe. *J. Am. Chem. Soc.* **1996**, *118*, 6317−6318.
(38) Lu, X.; Gopalakrishna, T. Y.; Phan, H.; Herng, T. S.; Jiang, Q.; Liu, C.; Li, G.; Ding, J.; Wu, J. Global Aromaticity in Macrocyclic Cyclopenta-Fused Tetraphenanthrenylene Tetraradicaloid and Its Charged Species. *Angew. Chem.* **2018**, *130*, 13236−13240.
(39) Fliegl, H.; Sundholm, D.; Taubert, S.; Pichierri, F. Aromatic Pathways in Twisted Hexaphyrins. *J. Phys. Chem. A* **2010**, *114*, 7153−7161.
(40) Huang, W.; Sergeeva, A. P.; Zhai, H.-J.; Averkiev, B. B.; Wang, L.-S.; Boldyrev, A. I. A concentric planar doubly π-aromatic B19− cluster. *Nat. Chem.* **2010**, *2*, 202−206.

https://doi.org/10.1021/acs.joc.1c00439
J. Org. Chem. 2021, 86, 6665−6673